

REAL COORDINATE STRETCHING PERFECTLY MATCHED LAYER FOR ANISOTROPIC ADVECTION-DIFFUSION EQUATION

AHMED BENMEFTAH^{1*}, NASSIMA KHALDI² and ZOHRA BENKAMRA²

ABSTRACT. We propose a real coordinate transformation for truncating an unbounded domain to numerically solve the anisotropic advection-diffusion equation. By replacing the complex stretching with a real variant, our method eliminates auxiliary variables and maintains well-posedness. Key advantages include: (1) analytical solutions via Laplace-Fourier transforms, (2) exact handling of anisotropy through diffusion tensor diagonalization, and (3) reduced computational cost in higher dimensions. The approach is validated for 2D anisotropic problems with cross-derivatives, offering a better alternative to frequency-dependent domain truncation techniques.

Keywords. Anisotropy, advection-diffusion, real coordinate stretching, PML, Green kernel

2020 Mathematics Subject Classification. Primary 65M85; Secondary 35M10, 35A08, 35B35

1. INTRODUCTION

Advection-diffusion equation is fundamental across a wide range of disciplines, from oceanography and meteorology to biomedical engineering and hydrology, especially when modeling large-scale phenomena in unbounded domains. In such cases, numerical simulations must incorporate artificial or open boundaries to accurately represent far-field solutions in real time. Among the primary techniques for constructing these boundaries, we can cite Absorbing Boundary Conditions (ABCs) which stand out as a key approach to truncating infinite domains [9, 19, 5, 3, 14, 7, 4, 15] and those that truncate them by absorbing layers of finite width such as Perfectly Matched Layers (PML)[1, 2]. Despite extensive research on domain truncation methods for wave propagation problems, there is (to the authors' knowledge) a notable scarcity of results in the numerical analysis literature concerning domain truncation construction methods for (mixed) advection-diffusion phenomena, especially in the presence of cross derivatives. Several significant studies have addressed boundary treatments for these equations.

Date: Received: Dec 24, 2025; Revised: Jan 18, 2026; Accepted: Jan 31, 2026.

* Corresponding author

© The Author(s) 2025. This article is licensed under a Creative Commons Attribution-NonCommercial-NoDerivatives 4.0 International License. To view a copy of the licence, visit <https://creativecommons.org/licenses/by-nc-nd/4.0/>.

For instance, [11, 13] developed a family of Artificial Boundary Conditions (ABCs) specifically for the advection-diffusion equation with small viscosity. In parallel, Halpern [13] investigated optimized sponge layers for convection-diffusion problems. Furthermore, [18] designed a PML formulation for heat and advection-diffusion equations, demonstrating that the reflection coefficient remains exponentially small relative to the layer width and damping parameter, regardless of the equation coefficients.

When considering the heat equation as a subcase of advection-diffusion, ABCs have historically been derived via continuous [16, 10, 12, 6] or discrete [8] approaches. A major limitation in these methods, stemming from the methodology in [9], is the necessity to approximate the square root of a partial differential operator. Conversely, the PML approach circumvents this issue by embedding the computational domain within a finite, non-reflexive dissipative layer. This technique effectively enforces the decay of outgoing waves without requiring complex operator approximations. They can be interpreted as a complex coordinate transformation, where spatial variables are analytically continued in the complex plane $x \mapsto x + 1/i\omega \int_0^x \sigma(s)ds$ through an absorption profile $\sigma \geq 0$, and ω is a time frequency. However, this seems to be specific to propagation problems, since an oscillatory frequency ω is tracked, making them more suitable for hyperbolic equations such as the wave or Maxwell equations [1, 2]. Furthermore, the factor $1/\omega$, which corresponds to an integral operator in the time domain, needs the introduction of auxiliary variables. This increases the computational cost and memory requirements, a problem that becomes particularly severe in higher dimensions.

In this work, we avoid this time inversion by introducing a simplified real coordinate transformation where spatial variables remain analytically continued into the real plane: $x \mapsto x + \int_0^x \sigma(s)ds$ which is by construction independent of ω and is henceforth very practical for computational implementation even in higher dimensions. Its main advantages are analyticity of fundamental solution, capability with corner layers and well-posedness which are simply inherited from the original equation. In addition, full anisotropy is carried out via a change of variable which allows one to suppress it from the equation in a new coordinate system and to obtain analytical Green Kernel in order to analyze the full decomposition of the total field into incident, reflected and transmitted parts.

The paper is structured as follows: Section 2 is dedicated to the derivation of a vertical layer model for the fully anisotropic advection-diffusion equation. This construction considers a spatiotemporal Dirac source positioned inside a nested subdomain. The solution without advection is obtained in Section 3 in Laplace-Fourier space, based on a suitable change of variable that keeps the normal direction invariant as needed in PML techniques and, at the same time, eliminates the cross derivatives, allowing the diagonalization of the diffusion tensor in the new coordinates. In Section 4, we return the solution back to the time-domain and show the decomposition of the total field into incident, reflected, and transmitted components. In Section 5, we recover a time-domain solution with advection with the help of a Galilean transformation. In Section 6, we rewrite the solution in original coordinates, and in Section 7 the RCSPML model is stated in all directions

and ready to be numerically validated in Section 8. Remarks and comments are discussed in the last section.

The two dimensional anisotropic advection-diffusion equation describes the transport of a scalar quantity $u(x, y, t)$ under both directional drift and anisotropic spreading, for which there are only vanishing modes. Its general form with a point source is given by:

$$\frac{\partial u}{\partial t} + \mathbf{v} \cdot \nabla u = \nabla \cdot (\mathbf{D} \nabla u) + \delta(\mathbf{x} - \mathbf{x}_0) \delta(t), \quad (1.1)$$

where: $\mathbf{v} = (v_x, v_y)$ is the velocity vector of advection and

$$\mathbf{D} = \begin{pmatrix} D_{xx} & \frac{D_{xy}}{2} \\ \frac{D_{xy}}{2} & D_{yy} \end{pmatrix}$$

is the diffusion tensor, \mathbf{x}_0 is the source location, δ represents the Dirac delta function.

If we consider a source located at $(h, 0)$, expanding in Cartesian coordinates yields:

$$\frac{\partial u}{\partial t} + v_x \frac{\partial u}{\partial x} + v_y \frac{\partial u}{\partial y} = D_{xx} \frac{\partial^2 u}{\partial x^2} + D_{xy} \frac{\partial^2 u}{\partial x \partial y} + D_{yy} \frac{\partial^2 u}{\partial y^2} + \delta(x - h) \delta(y) \delta(t). \quad (1.2)$$

for which the fundamental solution is given by

$$u(x, y, t) = \frac{H(t)}{2\pi t \sqrt{4D_{xx}D_{yy} - D_{xy}^2}} \exp\left(-\frac{\mathcal{Q}(x, y, t)}{2t(4D_{xx}D_{yy} - D_{xy}^2)}\right), \quad (1.3)$$

where the quadratic form $\mathcal{Q}(x, y, t)$ is:

$$\mathcal{Q}(x, y, t) = 2D_{yy}(x - x_0 - v_x t)^2 - 2D_{xy}(x - h - v_x t)(y - v_y t) + 2D_{xx}(y - v_y t)^2, \quad (1.4)$$

and $H(t)$ is the Heaviside step function enforcing causality. The center of the solution moves with velocity $\mathbf{v} = (v_x, v_y)$, and the anisotropic spreading is controlled by \mathbf{D} . For well posedness of the parabolic equation, one requires positive-definiteness of the quadratic form \mathcal{Q} , i.e., positives D_{xx} and D_{yy} and $4D_{xx}D_{yy} - D_{xy}^2 > 0$, positive-definite \mathbf{D} . Since there are only vanishing modes without temporal oscillation, a natural way to design a perfectly matched layer is to not incorporate the time frequency $i\omega$ in the coordinate stretching, such as in wave phenomena where the spatial coordinate (for example, in the x direction) is modified in Fourier space by the complex variable $X(x)$, so that $X(0) = 0$, and

$$x \mapsto X = x + \frac{1}{i\omega} \int_0^x \sigma(\tau) d\tau, \quad (1.5)$$

$\sigma \geq 0$ being the absorption profile. Instead, our strategy in this paper consists in introducing a real coordinate stretching defined by

$$x \mapsto X = x + \int_0^x \sigma(s) ds \quad (1.6)$$

which is by construction independent of the temporal frequency ω . In terms of partial derivatives, one can write:

$$\frac{\partial}{\partial X} = (1 + \sigma(x))^{-1} \frac{\partial}{\partial x} = \gamma(x) \frac{\partial}{\partial x}, \quad \gamma(x) := (1 + \sigma(x))^{-1}. \quad (1.7)$$

In this way, the layer will not be fictive. It becomes a real medium with the desired absorption and perfect matching properties. Since there is no time convolution, the PML equations will be completely free of auxiliary variables, which reduces significantly the computation cost in practice and allowing to solve multidimensional problems with very low complexity compared to Berenger's PMLs used in the literature for wave problems. In addition, the most tractable feature of such a method is the possibility to obtain an analytical solution very easily using the Fourier-Laplace transform, allowing us to fully describe reflected and transmitted fields and study the reflection coefficient as a function of the width and rate of absorption of the layer.

2. DESIGN OF REAL COORDINATE STRETCHING PERFECTLY MATCHED LAYER (RCSPML)

Consider the two-dimensional ($2d$) anisotropic heat equation with a finite layer of width L in the region $-L < x < 0$ where the change of variable (1.6) is used. A Dirac delta source in the nested region $x > 0$ is located at $(h, 0)$, $h > 0$, in space and $t = 0$ in time, with a variable absorption profile: $\sigma(x) \geq 0$ for $-L < x < 0$ and equal 0 for $x > 0$, regardless of the specific value of σ at the interface $x = 0$. Then, one has to find a causal solution to the following equations:

- **Nested region** ($x > 0$):

$$\frac{\partial u}{\partial t} + v_x \frac{\partial u}{\partial x} + v_y \frac{\partial u}{\partial y} = D_{xx} \frac{\partial^2 u}{\partial x^2} + D_{xy} \frac{\partial^2 u}{\partial x \partial y} + D_{yy} \frac{\partial^2 u}{\partial y^2} + \delta(x - h) \delta(y) \delta(t). \quad (2.1)$$

- **RCSPML region** ($-L < x < 0$):

$$\frac{\partial U}{\partial t} + v_x \frac{\partial U}{\partial X} + v_y \frac{\partial U}{\partial y} = D_{xx} \frac{\partial^2 U}{\partial X^2} + D_{xy} \frac{\partial^2 U}{\partial X \partial y} + D_{yy} \frac{\partial^2 U}{\partial y^2}, \quad (2.2)$$

where X is the real coordinate stretching given by (1.6) and $U(X, y, t) := u(x, y, t)$.

- **Interface conditions** at $x = 0$ (denoting $\sigma_0 = \sigma(0) \geq 0$ then $\gamma(0) = (1 + \sigma_0)^{-1}$):

$$u(0, y, t) = U(0, y, t), \quad \left. \frac{\partial u}{\partial x} \right|_{x=0} = \left. \frac{\partial U}{\partial X} \right|_{X=0} = \gamma(0) \left. \frac{\partial u}{\partial x} \right|_{x=0}. \quad (2.3)$$

- **Boundary conditions:** Dirichlet at $x = -L$:

$$u(-L, y, t) = U(X(-L), y, t) = 0. \quad (2.4)$$

Equation (2.2) becomes with the change of partial derivative (1.7) a variable coefficient equation as follows:

$$\frac{\partial u}{\partial t} + v_x \gamma(x) \frac{\partial u}{\partial x} + v_y \frac{\partial u}{\partial y} = D_{xx} \gamma(x) \frac{\partial}{\partial x} \gamma(x) \frac{\partial u}{\partial x} + D_{xy} \gamma(x) \frac{\partial^2 u}{\partial x \partial y} + D_{yy} \frac{\partial^2 u}{\partial y^2}. \quad (2.5)$$

However, for the computation of the fundamental solution, one does not need to deal with a variable-coefficient equation. This is because Equation (2.2) has constant coefficients in the coordinates (X, y) , making it more straightforward to solve than Equation (2.5).

3. LAPLACE-FOURIER-DOMAIN SOLUTION

Let \sqrt{z} denote the square root of a complex number z , with negative branch cut. We will solve our equation without the advective part, and then we will introduce the advection terms through a Galilean transformation. To eliminate the cross-derivative term, we introduce a change of variables that leaves the x -coordinate invariant.

$$\begin{cases} \xi = x, \\ \eta = y - \beta x, \end{cases} \quad \text{with } \beta = \frac{D_{xy}}{2D_{xx}}. \quad (3.1)$$

The preservation of the x -coordinate is essential for constructing the PML in this direction, as it ensures the interface and boundary conditions remain unchanged at $x = \xi = 0$ and $x = \xi = -L$, respectively.

Using the change of variables (3.1), we now introduce the following notations:

$$X(x) = x - \Sigma(x), \quad \Sigma(x) := \int_x^0 \sigma(q) dq.$$

$$U(X, \eta, t) = u(\xi, \eta, t), \quad X(\xi) = \xi - \int_\xi^0 \sigma(q) dq = \xi - \Sigma(\xi),$$

$$D_{\xi\xi} = D_{xx} > 0, \quad D_{\eta\eta} = \frac{4D_{xx}D_{yy} - D_{xy}^2}{4D_{xx}} > 0, \quad v_\xi = v_x, \quad v_\eta = v_y - \beta v_x,$$

we obtain the free cross-derivative equations as follows:

- **Nested region** ($\xi > 0$):

$$\frac{\partial u}{\partial t} + v_\xi \frac{\partial u}{\partial \xi} + v_\eta \frac{\partial u}{\partial \eta} = D_{\xi\xi} \frac{\partial^2 u}{\partial \xi^2} + D_{\eta\eta} \frac{\partial^2 u}{\partial \eta^2} + \delta(\xi - h)\delta(\eta + \beta h)\delta(t). \quad (3.2)$$

- **RCSPML region** ($-L < \xi < 0$):

$$\frac{\partial U}{\partial t} + v_\xi \frac{\partial U}{\partial X} + v_\eta \frac{\partial U}{\partial \eta} = D_{\xi\xi} \frac{\partial^2 U}{\partial X^2} + D_{\eta\eta} \frac{\partial^2 U}{\partial \eta^2}, \quad (3.3)$$

or, in terms of partial derivatives w.r.t (ξ, η) :

$$\frac{\partial u}{\partial t} + v_\xi \gamma(\xi) \frac{\partial u}{\partial \xi} + v_\eta \frac{\partial u}{\partial \eta} = D_{\xi\xi} \gamma(\xi) \frac{\partial}{\partial \xi} \gamma(\xi) \frac{\partial u}{\partial \xi} + D_{\eta\eta} \frac{\partial^2 u}{\partial \eta^2}. \quad (3.4)$$

Notice that the equations obtained in coordinates (ξ, η) are anisotropic free cross derivative. This will considerably simplify the computation of $2d$ Green kernels as a product of $1d$ kernels in a standard way as follows.

From now on, we denote by s the Laplace variable associated with time $t \geq 0$ and by k the (partial) Fourier variable associated to $\eta \in \mathbb{R}$. We will also use $\tilde{\phi}$ and $\hat{\phi}$ to denote the Laplace and Fourier transforms, respectively, of a tempered distribution $\phi(\xi, \eta, t)$ defined in $[-L, +\infty) \times \mathbb{R} \times \mathbb{R}^+$.

3.1. Nested Region ($\xi > 0$). Performing a partial Fourier transform in y followed by a Laplace transform in t of (3.2) respectively (without advective terms), one obtains an O.D.E in ξ with a Dirac source term as follows:

$$(s + D_{\eta\eta}k^2)\tilde{u}(\xi, k, s) - D_{\xi\xi}\tilde{u}''(\xi, k, s) = e^{ik\beta h}\delta(\xi - h)$$

for which the Laplace-Fourier domain solution is known:

$$\begin{aligned}\tilde{u}(\xi, k, s) &= \frac{1}{2\sqrt{D_{\xi\xi}(s + D_{\eta\eta}k^2)}}e^{-\sqrt{\frac{s+D_{\eta\eta}k^2}{D_{\xi\xi}}|\xi-h|}} \\ &\quad + Ae^{-\sqrt{\frac{s+D_{\eta\eta}k^2}{D_{\xi\xi}}\xi}} + Be^{+\sqrt{\frac{s+D_{\eta\eta}k^2}{D_{\xi\xi}}\xi}} \\ &= \frac{1}{2\sqrt{D_{\xi\xi}(s + D_{\eta\eta}k^2)}}e^{-\sqrt{\frac{s+D_{\eta\eta}k^2}{D_{\xi\xi}}|\xi-h|}} + Ae^{-\sqrt{\frac{s+D_{\eta\eta}k^2}{D_{\xi\xi}}\xi}},\end{aligned}$$

where $B = 0$, for a tempered distribution (slow growth at $+\infty$) and $A \neq 0$ will be determined by interface condition at $\xi = 0$ and/or boundary condition at $\xi = -L$.

3.2. RCSPML Region ($-L < \xi < 0$). In the layer region, there is no source, so the general solution to the homogeneous equation (3.3) (without advective terms) is given by:

$$\tilde{U}(X, k, s) = Ce^{-\sqrt{\frac{s+D_{\eta\eta}k^2}{D_{\xi\xi}}X}} + De^{+\sqrt{\frac{s+D_{\eta\eta}k^2}{D_{\xi\xi}}X}},$$

or using $\tilde{u}(\xi, k, s)$,

$$\tilde{u}(\xi, k, s) = Ce^{-\sqrt{\frac{s+D_{\eta\eta}k^2}{D_{\xi\xi}}(\xi-\Sigma(\xi))}} + De^{+\sqrt{\frac{s+D_{\eta\eta}k^2}{D_{\xi\xi}}(\xi-\Sigma(\xi))}},$$

where, $\xi - \Sigma(\xi) < 0$ for $-L < \xi < 0$. The coefficients C and D are determined by the interface conditions (2.3) and the boundary condition at $\xi = -L$.

3.3. Interface Matching. At $\xi = 0$, continuity of u and flux are given by interface conditions (2.3) and the Dirichlet boundary condition at $\xi = -L$. Solving three equations with three unknowns A, C, D , we obtain:

$$A = C = -\frac{e^{\sqrt{\frac{s+D_{\eta\eta}k^2}{D_{\xi\xi}}(-h-2L-2\Sigma(-L))}}}{2\sqrt{D_{\xi\xi}(s + D_{\eta\eta}k^2)}}, \quad D = \frac{e^{-\sqrt{\frac{s+D_{\eta\eta}k^2}{D_{\xi\xi}}h}}}{2\sqrt{D_{\xi\xi}(s + D_{\eta\eta}k^2)}}.$$

Therefore, in the nested domain ($\xi > 0$):

$$\tilde{u}(\xi, k, s) = \frac{e^{-\sqrt{\frac{s+D_{\eta\eta}k^2}{D_{\xi\xi}}|\xi-h|}}}{2\sqrt{D_{\xi\xi}(s + D_{\eta\eta}k^2)}} - \frac{e^{\sqrt{\frac{s+D_{\eta\eta}k^2}{D_{\xi\xi}}(-\xi-h-2L-2\Sigma(-L))}}}{2\sqrt{D_{\xi\xi}(s + D_{\eta\eta}k^2)}}, \quad (3.5)$$

and in the layer region ($-L < \xi < 0$):

$$\tilde{u}(\xi, k, s) = -\frac{e^{\sqrt{\frac{s+D_{\eta\eta}k^2}{D_{\xi\xi}}(-\xi-h-2L+\Sigma(\xi)-2\Sigma(-L))}}}{2\sqrt{D_{\xi\xi}(s + D_{\eta\eta}k^2)}} + \frac{e^{\sqrt{\frac{s+D_{\eta\eta}k^2}{D_{\xi\xi}}(-h+\xi-\Sigma(\xi))}}}{2\sqrt{D_{\xi\xi}(s + D_{\eta\eta}k^2)}}. \quad (3.6)$$

4. TIME-DOMAIN SOLUTION AND THE IMAGE PRINCIPLE

Now, one can use the inverse Laplace transform followed by the inverse Fourier transform to get the time domain solution in both the nested and layer regions as follows.

4.1. Nested region ($\xi > 0$).

4.1.1. *Time-Fourier-Domain Solution.* Performing the inverse Laplace transform, one has:

$$\begin{aligned}\hat{u}(\xi, k, t) &= \mathcal{L}^{-1} \left\{ \frac{1}{2\sqrt{D_{\xi\xi}(s + D_{\eta\eta}k^2)}} e^{-\sqrt{\frac{s+D_{\eta\eta}k^2}{D_{\xi\xi}}|\xi-h|} \right\} \\ &+ \mathcal{L}^{-1} \left\{ -\frac{e^{\sqrt{\frac{s+D_{\eta\eta}k^2}{D_{\xi\xi}}(-\xi-h-2L-2\Sigma(-L))}}}{2\sqrt{D_{\xi\xi}(s + D_{\eta\eta}k^2)}} \right\} \\ &= \frac{e^{-D_{\eta\eta}k^2t}}{2\sqrt{D_{\xi\xi}\pi t}} \left(e^{-\frac{(\xi-h)^2}{4D_{\xi\xi}t}} - e^{-\frac{(\xi+h+2L+2\Sigma(-L))^2}{4D_{\xi\xi}t}} \right).\end{aligned}$$

Expanding on this, we obtain the following.

$$\hat{u}(\xi, k, t) = \frac{1}{2\sqrt{D_{\xi\xi}\pi t}} e^{-D_{\eta\eta}k^2t - \frac{(\xi-h)^2}{4D_{\xi\xi}t}} - \frac{1}{2\sqrt{D_{\xi\xi}\pi t}} e^{-D_{\eta\eta}k^2t - \frac{(\xi+h+2L+2\Sigma(-L))^2}{4D_{\xi\xi}t}}.$$

4.1.2. *Time-Domain Solution.* Now, inverting the Fourier transform, one obtains the following.

$$\begin{aligned}u(\xi, \eta, t) &= \frac{1}{2\pi} \int_{-\infty}^{\infty} \left[\frac{e^{-D_{\eta\eta}k^2t}}{2\sqrt{D_{\xi\xi}\pi t}} \left(e^{-\frac{(\xi-h)^2}{4D_{\xi\xi}t}} - e^{-\frac{(\xi+h+2L+2\Sigma(-L))^2}{4D_{\xi\xi}t}} \right) \right] e^{ik\eta} dk \\ &= \frac{1}{2\pi} \frac{1}{2\sqrt{D_{\xi\xi}\pi t}} \left(e^{-\frac{(\xi-h)^2}{4D_{\xi\xi}t}} - e^{-\frac{(\xi+h+2L+2\Sigma(-L))^2}{4D_{\xi\xi}t}} \right) \int_{-\infty}^{\infty} e^{-D_{\eta\eta}tk^2} e^{ik\eta} dk \\ &= \frac{1}{4\pi t \sqrt{D_{\xi\xi}D_{\eta\eta}}} \left(e^{-\frac{(\xi-h)^2}{4D_{\xi\xi}t}} - e^{-\frac{(\xi+h+2L+2\Sigma(-L))^2}{4D_{\xi\xi}t}} \right) e^{-\frac{(\eta+\beta h)^2}{4D_{\eta\eta}t}}.\end{aligned}$$

Expanding, the last expression yields the following expression.

$$\begin{aligned}u(\xi, \eta, t) &= \frac{e^{-\left(\frac{(\xi-h)^2}{4D_{\xi\xi}t} + \frac{(\eta+\beta h)^2}{4D_{\eta\eta}t}\right)}}{4\pi t \sqrt{D_{\xi\xi}D_{\eta\eta}}} - \frac{e^{-\left(\frac{(\xi+h+2L+2\Sigma(-L))^2}{4D_{\xi\xi}t} + \frac{(\eta+\beta h)^2}{4D_{\eta\eta}t}\right)}}{4\pi t \sqrt{D_{\xi\xi}D_{\eta\eta}}} \\ &= \frac{e^{-\left(\frac{(\xi-h)^2}{4D_{\xi\xi}t} + \frac{(\eta+\beta h)^2}{4D_{\eta\eta}t}\right)}}{4\pi t \sqrt{D_{\xi\xi}D_{\eta\eta}}} - \frac{e^{-\left(\frac{(\xi+h+2L)^2}{4D_{\xi\xi}t} + \frac{(\eta+\beta h)^2}{4D_{\eta\eta}t}\right)}}{4\pi t \sqrt{D_{\xi\xi}D_{\eta\eta}}} \underbrace{e^{-\frac{\Sigma(-L)^2 + (\xi+h+2L)\Sigma(-L)}{D_{\xi\xi}t}}}_{:=R} \quad (4.1)\end{aligned}$$

where R is a reflection coefficient of the layer that can be written in terms of the mean absorption rate

$$\bar{\sigma} := \frac{\Sigma(-L)}{L} = \frac{1}{L} \int_{-L}^0 \sigma(\tau) d\tau. \quad (4.2)$$

Observe that this result is coherent with the image principle for the Dirichlet boundary condition at $\xi = -L$ which creates an inverse image source $-\delta(\xi^*)$ at the image point $(h^*, 0) = (-h - 2L, 0)$ symmetric to h w.r.t the axis $\xi = -L$. Let us denote by

$$G_{inc}(\xi, \eta, t) = \frac{e^{-\left(\frac{(\xi-h)^2}{4D_{\xi\xi}t} + \frac{(\eta+\beta h)^2}{4D_{\eta\eta}t}\right)}}{4\pi t \sqrt{D_{\xi\xi} D_{\eta\eta}}}$$

the incident Green kernel associated with the direct source at h , and

$$G_{inc}^*(\xi, \eta, t) := G_{inc}(\xi^*, \eta, t) = \frac{e^{-\left(\frac{(\xi+h+2L)^2}{4D_{\xi\xi}t} + \frac{(\eta+\beta h)^2}{4D_{\eta\eta}t}\right)}}{4\pi t \sqrt{D_{\xi\xi} D_{\eta\eta}}} \quad (4.3)$$

the inverse image incident Green kernel associated to the inverse image source at $(h^*, 0)$ with $\xi^* := \xi - h^* = \xi + h + 2L$ is the image point of ξ . Using this notation, the reflection coefficient takes the form

$$R_{L, \bar{\sigma}, h} = R_{L, \bar{\sigma}, h}(\xi, t) = e^{-\frac{L^2 \bar{\sigma}^2 + 2(\xi+h+2L)L\bar{\sigma}}{4D_{\xi\xi}t}}, \quad (4.4)$$

and the solution in the nested region $\xi > 0$ is splitted as an incident plus reflected fields as follows:

$$u(\xi, \eta, t) = G_{inc}(\xi, \eta, t) + G_{ref}(\xi, \eta, t),$$

where

$$G_{ref}(\xi, \eta, t) := R_{L, \bar{\sigma}, h}(\xi, t) G_{inc}^*(\xi, \eta, t) = -R_{L, \bar{\sigma}, h} \frac{e^{-\left(\frac{(\xi+h+2L)^2}{4D_{\xi\xi}t} + \frac{(\eta+\beta h)^2}{4D_{\eta\eta}t}\right)}}{4\pi t \sqrt{D_{\xi\xi} D_{\eta\eta}}} \quad (4.5)$$

is the reflected Green function by the layer of width L and absorption profile σ .

4.2. RCSPML Region ($-L < \xi < 0$).

4.2.1. *Time-Fourier-Domain Solution.* Similarly, inverting Laplace transform yields

$$\begin{aligned} \hat{u}(\xi, k, t) &= \mathcal{L}^{-1} \left\{ -\frac{e^{-\sqrt{\frac{s+D_{\eta\eta}k^2}{D_{\xi\xi}}}(\xi+h+2L+2\Sigma(-L)-\Sigma(\xi))}}{2\sqrt{D_{\xi\xi}(s+D_{\eta\eta}k^2)}} \right\} \\ &+ \mathcal{L}^{-1} \left\{ \frac{e^{-\sqrt{\frac{s+D_{\eta\eta}k^2}{D_{\xi\xi}}}(h-\xi+\Sigma(\xi))}}{2\sqrt{D_{\xi\xi}(s+D_{\eta\eta}k^2)}} \right\} \\ &= \frac{e^{-D_{\eta\eta}k^2 t}}{2\sqrt{D_{\xi\xi}\pi t}} \left(e^{-\frac{(h-\xi+\Sigma(\xi))^2}{4D_{\xi\xi}t}} - e^{-\frac{(\xi+h+2L-\Sigma(\xi)+2\Sigma(-L))^2}{4D_{\xi\xi}t}} \right). \end{aligned}$$

Expanding, we obtain:

$$\begin{aligned} \hat{u}(\xi, k, t) = & -\frac{1}{2\sqrt{D_{\xi\xi}\pi t}} e^{-D_{\eta\eta}k^2t - \frac{(\xi+h+2L-\Sigma(\xi)+2\Sigma(-L))^2}{4D_{\xi\xi}t}} \\ & + \frac{1}{2\sqrt{D_{\xi\xi}\pi t}} e^{-D_{\eta\eta}k^2t - \frac{(h-\xi+\Sigma(\xi))^2}{4D_{\xi\xi}t}}. \end{aligned} \quad (4.6)$$

4.2.2. *Time-Domain Solution.* Now, inverting Fourier transform:

$$\begin{aligned} u(\xi, \eta, t) = & \mathcal{F}^{-1} \left\{ \frac{e^{-D_{\eta\eta}k^2t}}{2\sqrt{D_{\xi\xi}\pi t}} \left(e^{-\frac{(h-\xi+\Sigma(\xi))^2}{4D_{\xi\xi}t}} - e^{-\frac{(\xi+h+2L-\Sigma(\xi)+2\Sigma(-L))^2}{4D_{\xi\xi}t}} \right) \right\} \\ = & \frac{1}{4\pi t \sqrt{D_{\xi\xi}D_{\eta\eta}}} \left(e^{-\frac{(h-\xi+\Sigma(\xi))^2}{4D_{\xi\xi}t}} - e^{-\frac{(\xi+h+2L-\Sigma(\xi)+2\Sigma(-L))^2}{4D_{\xi\xi}t}} \right) e^{-\frac{(\eta+\beta h)^2}{4D_{\eta\eta}t}}. \end{aligned}$$

Expanding the expression:

$$u(\xi, \eta, t) = \frac{e^{-\left(\frac{(h-\xi+\Sigma(\xi))^2}{4D_{\xi\xi}t} + \frac{(\eta+\beta h)^2}{4D_{\eta\eta}t}\right)}}{4\pi t \sqrt{D_{\xi\xi}D_{\eta\eta}}} - \frac{e^{-\left(\frac{(\xi+h+2L-\Sigma(\xi)+2\Sigma(-L))^2}{4D_{\xi\xi}t} + \frac{(\eta+\beta h)^2}{4D_{\eta\eta}t}\right)}}{4\pi t \sqrt{D_{\xi\xi}D_{\eta\eta}}}. \quad (4.7)$$

Likewise, this can be splitted as a sum of two transmitted fields: one from the direct source $(h, 0)$ in the nested region and the other from the image source $(h^*, 0)$ located in the image media and symmetric to $(h, 0)$ w.r.t $\xi = -L$, as follows:

$$\begin{aligned} u(\xi, \eta, t) = & \frac{e^{-\left(\frac{(h-\xi)^2}{4D_{\xi\xi}t} + \frac{(\eta+\beta h)^2}{4D_{\eta\eta}t}\right)}}{4\pi t \sqrt{D_{\xi\xi}D_{\eta\eta}}} \underbrace{e^{-\frac{\Sigma(\xi)^2 + (h-\xi)\Sigma(\xi)}{4D_{\xi\xi}t}}}_{:=T} \\ & - \frac{e^{-\left(\frac{(\xi+h+2L)^2}{4D_{\xi\xi}t} + \frac{(\eta+\beta h)^2}{4D_{\eta\eta}t}\right)}}{4\pi t \sqrt{D_{\xi\xi}D_{\eta\eta}}} \underbrace{e^{-\frac{(2\Sigma(-L)+\Sigma(\xi))^2 + 2(\xi+h+2L)(2\Sigma(-L)-\Sigma(\xi))}{4D_{\xi\xi}t}}}_{:=T^*} \end{aligned}$$

where the coefficients appearing in the r.h.s $T = T_{L,\bar{\sigma},h}$ and $T^* = T_{L,\bar{\sigma},h^*}$ are the transmission coefficients of the layer.

4.3. **Final solution for the anisotropic case without advection.** From subsections above, one can now write the anisotropic solution in both the nested and the layer regions in the case of zero advection and in the (ξ, η) as follows:

- In the physical domain ($\xi > 0$):

$$u(\xi, \eta, t) = \frac{e^{-\left(\frac{(\xi-h)^2}{4D_{\xi\xi}t} + \frac{(\eta+\beta h)^2}{4D_{\eta\eta}t}\right)}}{4\pi t \sqrt{D_{\xi\xi}D_{\eta\eta}}} - \frac{e^{-\left(\frac{(\xi+h+2L)^2}{4D_{\xi\xi}t} + \frac{(\eta+\beta h)^2}{4D_{\eta\eta}t}\right)}}{4\pi t \sqrt{D_{\xi\xi}D_{\eta\eta}}} \underbrace{e^{-\frac{\Sigma(-L)^2 + (\xi+h+2L)\Sigma(-L)}{D_{\xi\xi}t}}}_R$$

- In the RCSPML region ($-L < \xi < 0$):

$$u(\xi, \eta, t) = \frac{e^{-\left(\frac{(h-\xi)^2}{4D_{\xi\xi}t} + \frac{(\eta+\beta h)^2}{4D_{\eta\eta}t}\right)}}{4\pi t \sqrt{D_{\xi\xi}D_{\eta\eta}}} e^{\underbrace{-\frac{\Sigma(\xi)^2 + (h-\xi)\Sigma(\xi)}{4D_{\xi\xi}t}}_T} - \frac{e^{-\left(\frac{(\xi+h+2L)^2}{4D_{\xi\xi}t} + \frac{(\eta+\beta h)^2}{4D_{\eta\eta}t}\right)}}{4\pi t \sqrt{D_{\xi\xi}D_{\eta\eta}}} e^{\underbrace{-\frac{(2\Sigma(-L)+\Sigma(\xi))^2 + 2(\xi+h+2L)(2\Sigma(-L)-\Sigma(\xi))}{4D_{\xi\xi}t}}_{T^*}}.$$

In terms of reflection / transmission coefficients (see Figure 1), one thus has a reflected field in the nested region and two transmitted ones in the layer:

$$u(\xi, \eta, t) = \begin{cases} G_{inc}(\xi, \eta, t) + R G_{inc}^*(\xi, \eta, t) & \text{in the nested region, } \xi > 0 \\ T G_{inc}(\xi, \eta, t) + T^* G_{inc}^*(\xi, \eta, t) & \text{in the layer region, } -L < \xi < 0 \end{cases}$$

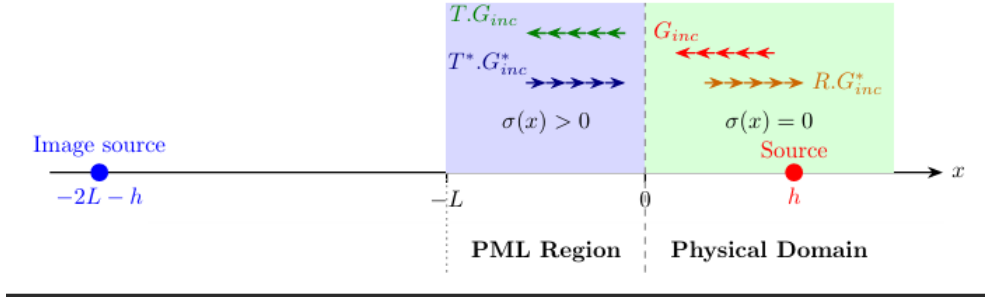


FIGURE 1. RCSPML interface showing the physical source at $x = h$, its image source at $x = -2L - h$, and the four field components: incident (G_{inc}), reflected (R), direct transmitted (T) and inverse image transmitted (T^*). The RCSPML region ($-L < x < 0$) with absorption profile $\sigma(x) > 0$.

5. TIME-DOMAIN SOLUTION WITH ADVECTION AND THE PERFECT MATCHING PROPERTY

Transforming back to the original frame, the solution of the advection diffusion equation with RCSPML can be deduced from the previous result, by considering a moving source located at $h(t) = h + v_{\xi}t$, $\eta \in \mathbb{R}$. The image source moves

henceforth in the opposite direction $h^*(t) = -h - v_\xi t - 2L$, $\eta \in \mathbb{R}$.

$$u(\xi, \eta, t) = \begin{cases} \frac{e^{-\left(\frac{(h+v_\xi t-\xi)^2}{4D_{\xi\xi}t} + \frac{(\eta-v_\eta t+\beta h)^2}{4D_{\eta\eta}t}\right)}}{4\pi t \sqrt{D_{\xi\xi}D_{\eta\eta}}} & \\ \frac{e^{-\left(\frac{(h+v_\xi t+\xi+2L+2\Sigma(-L))^2}{4D_{\xi\xi}t} + \frac{(\eta-v_\eta t+\beta h)^2}{4D_{\eta\eta}t}\right)}}{4\pi t \sqrt{D_{\xi\xi}D_{\eta\eta}}} & \text{if } \xi > 0 \\ \frac{e^{-\left(\frac{(h+v_\xi t-\xi+\Sigma(\xi))^2}{4D_{\xi\xi}t} + \frac{(\eta-v_\eta t+\beta h)^2}{4D_{\eta\eta}t}\right)}}{4\pi t \sqrt{D_{\xi\xi}D_{\eta\eta}}} & \\ \frac{e^{-\left(\frac{(h+v_\xi t+\xi+2L-\Sigma(\xi)+2\Sigma(-L))^2}{4D_{\xi\xi}t} + \frac{(\eta-v_\eta t+\beta h)^2}{4D_{\eta\eta}t}\right)}}{4\pi t \sqrt{D_{\xi\xi}D_{\eta\eta}}} & \text{if } -L < \xi < 0. \end{cases}$$

In terms of reflection / transmission coefficients:

$$u(\xi, \eta, t) = \begin{cases} G_{inc}(\xi, \eta, t) + R G_{inc}^*(\xi, \eta, t) & \text{in the physical region, } \xi > 0 \\ T G_{inc}(\xi, \eta, t) + T^* G_{inc}^*(\xi, \eta, t) & \text{in the RCSPML region, } -L < \xi < 0 \end{cases}$$

where G_{inc} and G_{inc}^* are the Green functions associated to the moving source at $(h(t), 0) = (h + v_\xi t, 0)$ and the inverse image source at $(h^*(t), 0) = (-h - 2L - v_\xi t, 0)$ respectively. $R = R_{L, \bar{\sigma}, h, v_\xi}(\xi, t)$ represents the reflection coefficient of the layer.

$$R_{L, \bar{\sigma}, h, v_\xi}(\xi, t) = e^{-\frac{L^2 \bar{\sigma}^2 + (\xi + h + v_\xi t + 2L)L\bar{\sigma}}{D_{\xi\xi}t}}$$

T and T^* are left and right transmission coefficients, respectively:

$$T_{L, \bar{\sigma}, h, v_\xi}(\xi, t) = e^{-\frac{\Sigma(\xi)^2 + (h - \xi - v_\xi t)\Sigma(\xi)}{4D_{\xi\xi}t}}$$

$$T_{L, \bar{\sigma}, h, v_\xi}^*(\xi, t) = e^{-\frac{(2L\bar{\sigma} + \Sigma(\xi))^2 + 2(\xi + h - v_\xi t + 2L)(2L\bar{\sigma} - \Sigma(\xi))}{4D_{\xi\xi}t}}$$

It follows immediately that at a fixed time $t > 0$:

- (1) Even with σ constant ($\bar{\sigma} = \sigma_0 > 0$), the layer ($L = +\infty$) is perfectly matched at any $\xi \geq 0$, in particular, at $\xi = 0$, in fact: $R_{\infty, \sigma_0, h, v_\xi}(0, t) = T_{\infty, \sigma_0, h, v_\xi}^*(0, t) = 0$, $T_{\infty, \sigma_0, h, v_\xi}(0, t) = 1$.
- (2) In the case of finite layer of width $L > 0$, perfect matching can be reached by:
 - (a) allowing an unbounded profile σ in such a way that $\bar{\sigma} = +\infty$ and one obtains: $R_{L, \infty, h, v_\xi}(0, t) = T_{L, \infty, h, v_\xi}^*(0, t) = 0$, $T_{L, \infty, h, v_\xi}(0, t) = 1$.
 - (b) or by the most common way of choice of polynomial profile (generally quadratic) in order to achieve a balance between perfect matching and discrete reflection coefficient that minimizes spurious reflection due to the grid resolution.

Remark 5.1. Observe that, while the pure heat kernel has only polynomial decay in time as $O(t^{-1})$ as $t \rightarrow +\infty$, the advection kernel has an exponential decay

$O(t^{-1}e^{-\frac{v_\xi t}{4D_{\xi\xi}}})$ as $t \rightarrow +\infty$, as soon as $v_\xi \neq 0$. This regularizing effect brings actually a great advantage to the precision of the RCSPML over long periods.

6. ANISOTROPIC SOLUTION IN ORIGINAL COORDINATES (x, y)

Recall the transformation between (ξ, η) and (x, y) coordinates is given by:

$$\xi = x, \quad (6.1)$$

$$\eta = y - \beta x, \quad \text{where } \beta = \frac{D_{xy}}{2D_{xx}}, \quad (6.2)$$

with the transformed parameters:

$$D_{\xi\xi} = D_{xx} > 0, \quad (6.3)$$

$$D_{\eta\eta} = \frac{4D_{xx}D_{yy} - D_{xy}^2}{4D_{xx}} > 0, \quad (6.4)$$

$$v_\xi = v_x, \quad (6.5)$$

$$v_\eta = v_y - \beta v_x. \quad (6.6)$$

We can present now the exact solution in the original coordinates (x, y) for the anisotropic advection-diffusion equation with cross derivatives and a RCSPML of width L placed at the left of the half-plane $x > 0$, as follows:

- **Nested region** ($x > 0$):

$$u_{\text{right}}(x, y, t) = \frac{1}{2\pi t \sqrt{4D_{xx}D_{yy} - D_{xy}^2}} \left[\exp\left(-\frac{(x - v_x t - h)^2}{4D_{xx}t}\right) - \exp\left(-\frac{(x + v_x t + h + 2L(1 + \bar{\sigma}))^2}{4D_{xx}t}\right) \right] \exp\left(-\frac{\left(D_{xx}(y - v_y t) - \frac{D_{xy}}{2}(x - h - v_x t)\right)^2}{D_{xx}(4D_{xx}D_{yy} - D_{xy}^2)t}\right).$$

- **RCSPML region** ($-L < x < 0$):

$$u_{\text{left}}(x, y, t) = \frac{1}{2\pi t \sqrt{4D_{xx}D_{yy} - D_{xy}^2}} \left[\exp\left(-\frac{(x - h - v_x t - \Sigma(x))^2}{4D_{xx}t}\right) - \exp\left(-\frac{(x + h + v_x t + 2L(1 + \bar{\sigma}) - \Sigma(x))^2}{4D_{xx}t}\right) \right] \exp\left(-\frac{\left(D_{xx}(y - v_y t) - \frac{D_{xy}}{2}(x - h - v_x t)\right)^2}{D_{xx}(4D_{xx}D_{yy} - D_{xy}^2)t}\right).$$

It is obvious that, by construction, $\Sigma(0) = 0$ implies directly $u_{\text{right}}(0^+, x, t) = u_{\text{left}}(0^-, y, t)$ which yields continuity of the solution at $x = 0$.

As a main result, the following theorem shows that reflections caused by the layer can be made as negligible as possible by choosing either a far source ($h \rightarrow +\infty$), a large layer ($L \rightarrow +\infty$) or enough absorption rate ($\bar{\sigma} \rightarrow +\infty$). Of course, the last alternative is the most common one used in practice.

Theorem 6.1. *The fundamental solution $u(x, y, t)$ is equivalent to the nested region solution $u_{\text{right}}(x, y, t)$ in the limit when h , L , or $\bar{\sigma}$ approaches $+\infty$. More precisely, when any of these parameters diverges, the solution reduces to:*

$$u_{\text{right}}(x, y, t) \xrightarrow{h, L \text{ or } \bar{\sigma} \rightarrow +\infty} u(x, y, t)$$

where $u(x, y, t)$ is the Green kernel in the free space given by (1.3).

Proof. The $H(t)$ in the fundamental solution is implicitly contained in u_{right} through its physical interpretation (causality). Analyzing the limit term by term, the nested solution contains two exponential terms. The second term

$$\exp\left(-\frac{(x + v_x t + h + 2L(1 + \bar{\sigma}))^2}{4D_{xx}t}\right)$$

disappears in the limit when any parameter h , L or $\bar{\sigma} \rightarrow +\infty$. Therefore, u_{right} reduces to:

$$\frac{1}{2\pi t \sqrt{4D_{xx}D_{yy} - D_{xy}^2}} \exp\left(-\frac{(x - v_x t - h)^2}{4D_{xx}t} - \frac{\left(D_{xx}(y - v_y t) - \frac{D_{xy}}{2}(x - h - v_x t)\right)^2}{D_{xx}(4D_{xx}D_{yy} - D_{xy}^2)t}\right).$$

The exponent can be rewritten as:

$$-\frac{1}{t} \left[\frac{(x - h - v_x t)^2}{4D_{xx}} + \frac{\left(D_{xx}(y - v_y t) - \frac{D_{xy}}{2}(x - h - v_x t)\right)^2}{D_{xx}(4D_{xx}D_{yy} - D_{xy}^2)} \right]$$

which exactly matches the quadratic form $\mathcal{Q}(x, y, t)$ in the fundamental solution when expanded as given by (1.4). Thus, we have shown that $u_{\text{right}}(x, y, t)$ converges point-wise to $u(x, y, t)$ in the specified limits. \square

7. THE RCSPML IN ALL DIRECTIONS

We can now define the equations to solve, in the case of a rectangular nested region completely surrounded by horizontal and vertical layers, respectively, as follows: In order to consider RCSPML in both the x and y directions, one must introduce the change of variable with absorption profiles σ_x and σ_y such that:

$$X(x) = x + \int_{\text{Interface}}^x \sigma_x(\tau) d\tau \text{ and } Y(y) = y + \int_{\text{Interface}}^y \sigma_y(\tau) d\tau$$

which amounts to changing the spatial derivatives by the corresponding rules:

$$\frac{\partial}{\partial x} \rightarrow \gamma_x(x) \frac{\partial}{\partial x}, \quad \gamma_x(x) := (1 + \sigma_x(x))^{-1},$$

$$\frac{\partial}{\partial y} \rightarrow \gamma_y(y) \frac{\partial}{\partial y}, \quad \gamma_y(y) := (1 + \sigma_y(y))^{-1}.$$

By this way, we obtain a variable coefficient equation which is free of any auxiliary unknown as follows:

$$\begin{aligned} \frac{\partial u}{\partial t} + v_x \gamma_x \frac{\partial u}{\partial x} + v_y \gamma_y \frac{\partial u}{\partial y} &= D_{xx} \gamma_x \frac{\partial}{\partial x} \gamma_x \frac{\partial u}{\partial x} + D_{xy} \gamma_x \gamma_y \frac{\partial^2 u}{\partial x \partial y} + D_{yy} \gamma_y \frac{\partial}{\partial y} \gamma_y \frac{\partial u}{\partial y} \\ &+ \delta(x-h) \delta(y) \delta(t). \end{aligned} \quad (7.1)$$

Clearly, if one assumes σ_x, σ_y to be zero outside the corresponding layers, then the (viscosity) coefficients γ_x, γ_y become equal to one outside their layers which reduces Equation (7.1) to the original advection-diffusion equation (2.1) in the nested region. In summary, the RCSPML system to solve in the free computational domain Ω can be written as follows: (Analytical solutions can be found by convolution)

- In the case of a Dirac source inside the nested region:

$$\left\{ \begin{array}{ll} \frac{\partial u}{\partial t} + v_x \gamma_x \frac{\partial u}{\partial x} + v_y \gamma_y \frac{\partial u}{\partial y} &= D_{xx} \gamma_x \frac{\partial}{\partial x} \gamma_x \frac{\partial u}{\partial x} + D_{xy} \gamma_x \gamma_y \frac{\partial^2 u}{\partial x \partial y} + D_{yy} \gamma_y \frac{\partial}{\partial y} \gamma_y \frac{\partial u}{\partial y} \\ &+ \delta(x-h) \delta(y) \delta(t) \\ \text{Continuity of } u \text{ and } \gamma_x \frac{\partial u}{\partial x}, &\text{at vertical interfaces} \\ \text{Continuity of } u \text{ and } \gamma_y \frac{\partial u}{\partial y}, &\text{at horizontal interfaces} \\ u = 0 \text{ on } \partial\Omega, &\text{Dirichlet B.C at outer boundary} \\ u(x, y, 0) = 0 \text{ on } \Omega, &\text{Zero initial condition at } t = 0. \end{array} \right.$$

- Or, in the case of an initial condition at $t = 0$, which is compactly supported in the nested region:

$$\left\{ \begin{array}{ll} \frac{\partial u}{\partial t} + v_x \gamma_x \frac{\partial u}{\partial x} + v_y \gamma_y \frac{\partial u}{\partial y} &= D_{xx} \gamma_x \frac{\partial}{\partial x} \gamma_x \frac{\partial u}{\partial x} + D_{xy} \gamma_x \gamma_y \frac{\partial^2 u}{\partial x \partial y} + D_{yy} \gamma_y \frac{\partial}{\partial y} \gamma_y \frac{\partial u}{\partial y} \\ \text{Continuity of } u \text{ and } \gamma_x \frac{\partial u}{\partial x}, &\text{at vertical interfaces} \\ \text{Continuity of } u \text{ and } \gamma_y \frac{\partial u}{\partial y}, &\text{at horizontal interfaces} \\ u = 0 \text{ on } \partial\Omega, &\text{Dirichlet B.C at outer boundary} \\ u(x, y, 0) = u_0(x, y) \text{ on } \Omega, &\text{initial condition at } t = 0. \end{array} \right. \quad (7.2)$$

Remark 7.1. Note that this model can be systematically extended to higher dimensions without introducing auxiliary variables. Namely, following the methodology of [17], this extension is also possible, with some technical modifications, for the time-fractional advection-diffusion equation. This represents a potential advantage over existing PML formulations for advection-diffusion equations found in the literature.

Remark 7.2 (Well-posedness and stability). It should be pointed out that the Cauchy problem (7.2) is a variable coefficients system in the coordinates (x, y) ,

but it is a constant coefficients one in the new coordinates (X, Y) . In fact, the system is originally equivalent to :

$$\left\{ \begin{array}{ll} \frac{\partial U}{\partial t} + v_x \frac{\partial U}{\partial X} + v_y \frac{\partial U}{\partial Y} & = D_{xx} \frac{\partial^2 U}{\partial X^2} + D_{xy} \frac{\partial^2 U}{\partial X \partial Y} + D_{yy} \frac{\partial^2 U}{\partial Y^2} \\ \text{Continuity of } U \text{ and } \frac{\partial U}{\partial X}, & \text{at vertical interfaces} \\ \text{Continuity of } U \text{ and } \frac{\partial U}{\partial Y}, & \text{at horizontal interfaces} \\ U = 0 \text{ on } \partial \tilde{\Omega}, & \text{Dirichlet B.C at outer boundary} \\ U(X, Y, 0) = U_0(X, Y) \text{ on } \tilde{\Omega}, & \text{initial condition at } t = 0, \end{array} \right.$$

where $\tilde{\Omega}$ is the image domain under the PML transformation $(x, y) \mapsto (X, Y)$ and $U(X, Y, t) := u(x, y, t)$. Notice that interfaces are invariant under the coordinate stretching, by construction.

It is well known that this constant Cauchy problem is well-posed and stable, as long as the diffusion tensor is positive definite, thus $\|U\|_{L^2(\tilde{\Omega})} \leq \|U_0\|_{L^2(\tilde{\Omega})}$, $\forall t > 0$.

On the other hand, $dx dy = \gamma_x \gamma_y dX dY$, $\gamma_x, \gamma_y \in (0, 1]$, then

$$\|u\|_{L^2(\Omega)} = \int_{\Omega} |u|^2 dx dy = \int_{\tilde{\Omega}} |U|^2 \gamma_x \gamma_y dX dY \leq \|U\|_{L^2(\tilde{\Omega})} \leq \|U_0\|_{L^2(\tilde{\Omega})},$$

with

$$\|U_0\|_{L^2(\Omega)} = \int_{\tilde{\Omega}} |U_0|^2 dX dY = \int_{\Omega} |u_0|^2 \frac{1}{\gamma_x \gamma_y} dx dy \leq \left\| \frac{1}{\gamma_x \gamma_y} \right\|_{L^\infty(\Omega)} \|u_0\|_{L^2(\Omega)}.$$

If σ_x and σ_y are assumed $L^\infty(\Omega)$, then $\frac{1}{\gamma_x} := 1 + \sigma_x$ and $\frac{1}{\gamma_y} := 1 + \sigma_y$ are also $L^\infty(\Omega)$. Thus $\|u\|_{L^2(\Omega)} \leq C \|u_0\|_{L^2(\Omega)}$, $\forall t > 0$. Henceforth, the stability and the well-posedness of the variable coefficients linear system (7.2) follows immediately.

In the following section, numerical results are conducted on this model Cauchy problem.

8. NUMERICAL RESULTS

Let us consider a particular initial condition in the frame xy , a $2d$ Gaussian distribution centered at $(0, 0)$ with standard deviations L_x and L_y in the x and y directions, respectively. The absence of D_{xy} (cross-diffusion) and v_x, v_y (drift terms) at $t = 0$ means that the initial condition is a separable Gaussian function:

$$u_0(x, y) = \frac{1}{2\pi L_x L_y} \exp\left(-\frac{x^2}{2L_x^2} - \frac{y^2}{2L_y^2}\right),$$

for which an analytical (or exact) solution is known:

$$u_{\text{Ex}}(x, y, t) = \frac{1}{2\pi\sqrt{(L_x^2 + 2D_{xx}t)(L_y^2 + 2D_{yy}t) - (D_{xy}t)^2}} \exp\left(-\frac{(L_y^2 + 2D_{yy}t)(x - v_x t)^2 + (L_x^2 + 2D_{xx}t)(y - v_y t)^2 - 2D_{xy}t(x - v_x t)(y - v_y t)}{2((L_x^2 + 2D_{xx}t)(L_y^2 + 2D_{yy}t) - (D_{xy}t)^2)}\right). \quad (8.1)$$

The analytical solution describes a $2d$ anisotropic Gaussian distribution evolving under diffusion and drift.

In the subsequent numerical tests, the computational domain is denoted by $\Omega_{L+d}^{\text{eff}} =] - (L + d) \times sd_{\text{eff}}, (L + d) \times sd_{\text{eff}}[$. This rectangular area consists of an inner subdomain $\Omega_L^{\text{eff}} =] - L \times sd_{\text{eff}}, L \times sd_{\text{eff}}[$, which is padded on all sides by a margin of width $d \times sd_{\text{eff}}$. Here, the parameter sd_{eff} represents the effective standard deviation associated with the anisotropic diffusion and the viscosity of the tensor D . If λ_1, λ_2 are the eigenvalues of D then sd_{eff} is given by:

$$sd_{\text{eff}} = \sqrt{2T\lambda_1\lambda_2} = \sqrt{2T}\sqrt{\det D}, \quad (8.2)$$

where T is the total simulation time. The quantities L and d are some reference length scales related to the standard deviations L_x and L_y of the initial Gaussian.

Denoting by $L_{\text{eff}} = L \times sd_{\text{eff}}$ and $d_{\text{eff}} = d \times sd_{\text{eff}}$, the RCSPML system we used is the one given by (7.2) that covers the horizontal, vertical, and corner layers. The absorption profile σ (representing σ_x or σ_y) is designed to be inversely proportional to the effective width d_{eff} and quadratic with respect to the distance from the domain interface. We define a normalized relative coordinate r and the profile function as follows:

$$r = \frac{|x| - L_{\text{eff}}}{d_{\text{eff}}} \in]0, 1[, \quad \sigma(x) = \frac{\sigma_{\text{max}}}{d_{\text{eff}}} r^2 \quad \text{for } L_{\text{eff}} < |x| < L_{\text{eff}} + d_{\text{eff}}.$$

In this definition, the variable x corresponds to vertical layers and should be substituted by y for horizontal ones. Based on empirical optimization, the value $\sigma_{\text{max}} = 50$ yields the most accurate numerical results.

The spatial domain is discretized using a uniform grid with spacing $\Delta x = \Delta y$. To advance the solution in time, we employ the explicit Forward in Time Centered in Space (FTCS) scheme. The time step Δt is selected to satisfy the CFL stability condition dictated by the physical parameters. We denote the resulting numerical approximation by u . Additionally, a reference solution, denoted as u_{ref} , is computed over the interval $[0, T]$ on an extended domain $\Omega_{\text{ref}} = \Omega_{4(L+d)}^{\text{eff}}$. This domain is enlarged fourfold to mitigate boundary effects.

In all the experiments bellow and unless some specific mentions, most key insights about the scheme parameters are summarized in Table 1.

Figures 2 and 6 show seismogram in time at two monitoring points. Top subplot: point near bottom-left corner (x_1, y_1) and bottom subplot: point near top-right corner (x_2, y_2) . Each of them shows: numerical solution (blue) and analytical solution (red dashed): We observe a smooth pulse arrival (earlier at (x_2, y_2) since

Category	Parameter/Formula	Value	Description
Initial condition	$L_x = L_y$	1	Standard deviation of the Gaussian pulse
Physics	$D = \begin{pmatrix} D_{xx} & \frac{D_{xy}}{2} \\ \frac{D_{xy}}{2} & D_{yy} \end{pmatrix}$	$\begin{pmatrix} 0.5 & 0.125 \\ 0.125 & 0.5 \end{pmatrix}$	Diffusion tensor
	$V = (v_x, v_y)$	(0.25, 0.25)	Advection field
Time	T	25	Total simulation time
Domain	$sd_{\text{eff}} = \sqrt{2T} \sqrt{\det D}$	4.92	The standard deviation incorporating the viscosity D and time T .
	$L + d$	$0.8 + 0.2 = 1$	Reference length
	Ω_L^{eff}	$] - 3.936, 3.936]^2$	Scaled Nested domain
	$\Omega_{L+d}^{\text{eff}}$	$] - 4.92, 4.92]^2$	Scaled Computational domain
	(x_1, y_1)	$(-3.1, -3.1)$	Receiver at bottom-left corner for seismogram
	(x_2, y_2)	$(3.1, 3.1)$	Receiver at top-right corner for seismogram
Grid	dt	0.0025	Time step size
	$\Delta x = \Delta y$	0.1	Space step size
	$N_x = N_y$	101	Number of grid-points in $\Omega_{L+d}^{\text{eff}}$
RCSPML (quadratic)	$d_{\text{eff}} = d \times sd_{\text{eff}}$	0.984	Scaled RCSPML width
	σ_{max}	50	Maximum absorption rate in both directions

TABLE 1. Parameters used in the FTCS numerical scheme

the field is advected right/up. The numerical pulses closely match the analytical one, for both reference cf. Figure 2 and RCSPML cf. Figure 6 solutions.

More precisely, to study the numerical precision w.r.t. the exact solution, we introduce the absolute error $\epsilon_*(x, y, t) = |u(x, y, t) - u_{\text{Ex}}(x, y, t)|$ in order to highlight the truncation of the effective nested region by either a far boundary to have a numerical reference solution ($* = \text{ref}$) or a Dirichlet Boundary Condition ($* = \text{DBC}$) or a RCSPML absorbing layer ($* = \text{RCSPML}$). In the effective nested domain Ω_L^{eff} , we compute the L^p ($p = 2$, and $p = \infty$) relative errors in percentage (%) over time in $[0, T]$, i.e.

$$e_*^p(t) := \frac{\|\epsilon_*(\cdot, \cdot, t)\|_p}{\|u_{\text{Ex}}(\cdot, \cdot, t)\|_p} \times 100\%, \quad * \in \{\text{ref}, \text{DBC}, \text{RCSPML}\}.$$

In the figures 3 and 7, semi-log plots show how numerical relative errors evaluate over time w.r.t the analytical solution in the nested domain, showing namely their maximum values at top of the pictures:

- L^2 Relative error (blue solid line): Measures average overall solution accuracy.
- L^∞ Relative error (red dashed line): Measures worst-case point-wise error.

Maximum values of the numerical relative errors are reported in Table 2: They Closely match for both reference and RCSPML solutions, while there is a large mismatch (high reflection) of the numerical solution obtained with a DBC to truncate the nested region.

Note that we can improve accuracy by two standard ways:

- (1) Increasing RCSPML Width: Recall that in the previous experiment (Table 2) we have used a width $d_{\text{eff}} = 0.984$. Tested with slightly larger widths $d_{\text{eff}} = 1.23$ and $d_{\text{eff}} = 1.476$ to reduce spurious reflections.

*	$\max e_*^2(\%)$	$\max e_*^\infty(\%)$
u_{ref}	0.12	0.19
u_{DBC}	93.02	100
u_{RCSPML}	0.41	1.28

TABLE 2. Maximum values of e_*^p (in %), for $p = \infty$ and $p = 2$. RCSPML width $d_{\text{eff}} = 0.984$

Maximum values of the numerical relative errors match more precisely for both reference and RCSPML solutions, as shown in the following Table 3. One observes that the maximum discretizations error is reached at $d_{\text{eff}} = 1.476$.

$d_{\text{eff}} = 1.23$ *	$\max e_*^2(\%)$	$\max e_*^\infty(\%)$	$d_{\text{eff}} = 1.476$ *	$\max e_*^2(\%)$	$\max e_*^\infty(\%)$
u_{ref}	0.12	0.19	u_{ref}	0.12	0.19
u_{RCSPML}	0.16	0.46	u_{RCSPML}	0.12	0.19

TABLE 3. Maximum values of e_*^p (in %), for $p = \infty$ and $p = 2$, for RCSPML widths $d_{\text{eff}} = 1.23$ (left table) and $d_{\text{eff}} = 1.476$ (right table).

- (2) Refining Spatial Mesh: With the RCSPML width fixed at $d_{\text{eff}} = 0.984$, we investigate the effect of spatial refinement by factors of **1.5** and **2**. The previous experiment (Table 2) used 101 and 401 grid points in both directions for the domains $\Omega_{L+d}^{\text{eff}}$ and $\Omega_{4(L+d)}^{\text{eff}}$ respectively, corresponding to a fixed grid spacing of $\Delta x = \Delta y = 0.1$.

After refinement, the grid resolutions become:

- 1.5 \times refinement: 151 and 601 points ($\Delta x = \Delta y = 0.0667$)
- 2 \times refinement: 201 and 801 points ($\Delta x = \Delta y = 0.05$)

for $\Omega_{L+d}^{\text{eff}}$ and $\Omega_{4(L+d)}^{\text{eff}}$ respectively.

As summarized in Table 4, the maximum relative errors decrease with mesh refinement for both solutions, u_{ref} and u_{RCSPML} , showing improved accuracy. Note that temporal refinement was not performed in this experiment.

Refinement $\times 1.5$ *	$\max e_*^2(\%)$	$\max e_*^\infty(\%)$	Refinement $\times 2$ *	$\max e_*^2(\%)$	$\max e_*^\infty(\%)$
u_{ref}	0.04	0.06	u_{ref}	0.02	0.03
u_{RCSPML}	0.04	0.08	u_{RCSPML}	0.03	0.03

TABLE 4. Maximum values of e_*^p (in %), for $p = \infty$ and $p = 2$, for refinement factor 1.5 (left table) and 2 (right table).

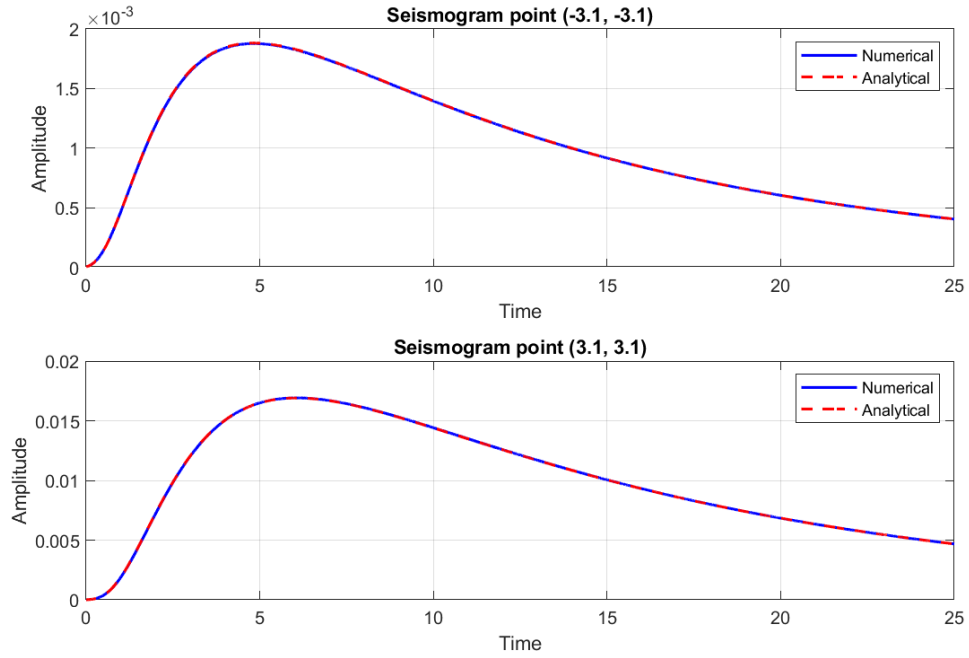


FIGURE 2. Time solution reference (numerical) v.s. analytical at two monitoring points: Top subplot: Point near bottom-left corner (x_1, y_1) , Bottom subplot: Point near top-right corner (x_2, y_2) .

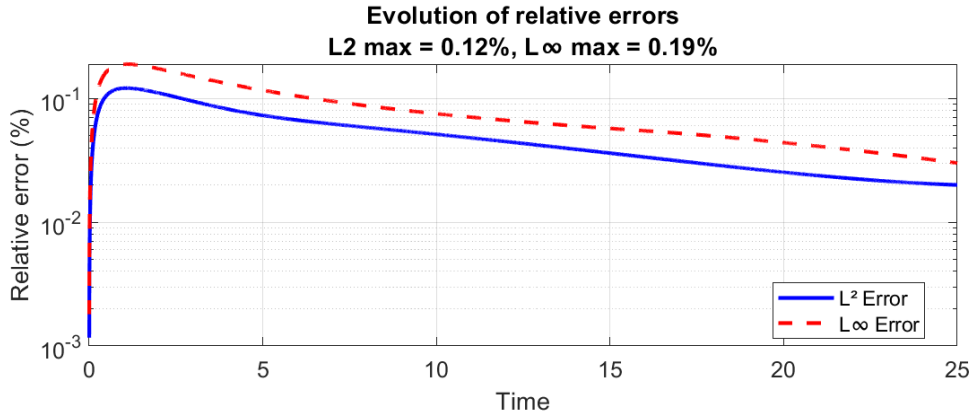


FIGURE 3. Semi-log plot over time: L^2 / L^∞ relative errors in percentage (%) of reference solution w.r.t analytical solution.

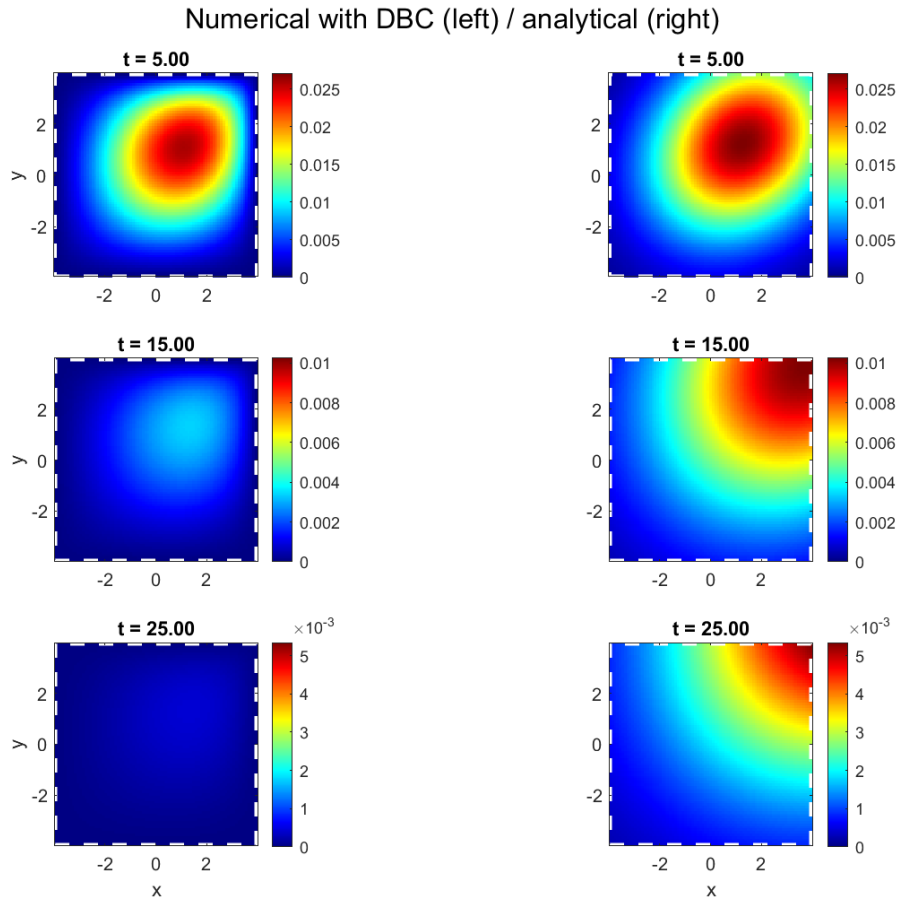


FIGURE 4. Snapshots comparison in the nested region Ω_L^{eff} (ended with Dirichlet B.C) between the numerical solution (left) and analytical solution (right) at three different times.

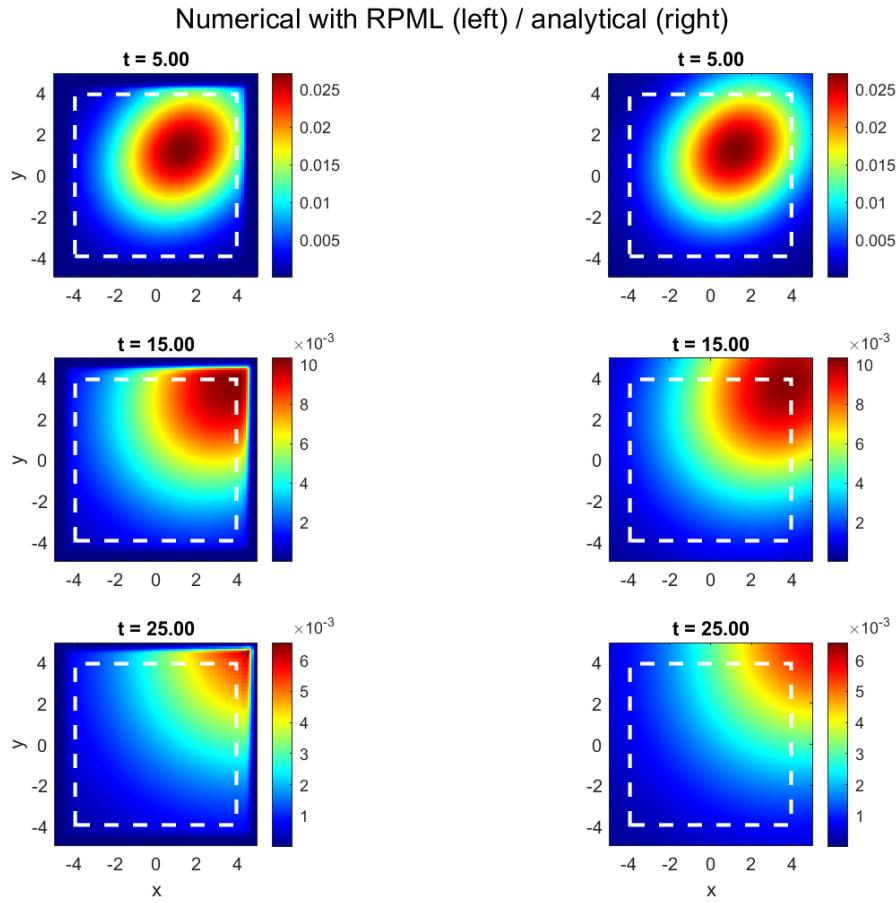


FIGURE 5. Snapshots comparison in the computational region $\Omega_{L+d}^{\text{eff}}$ (with RCSPML) between the RCSPML numerical solution (left) and analytical solution (right) at three different times.

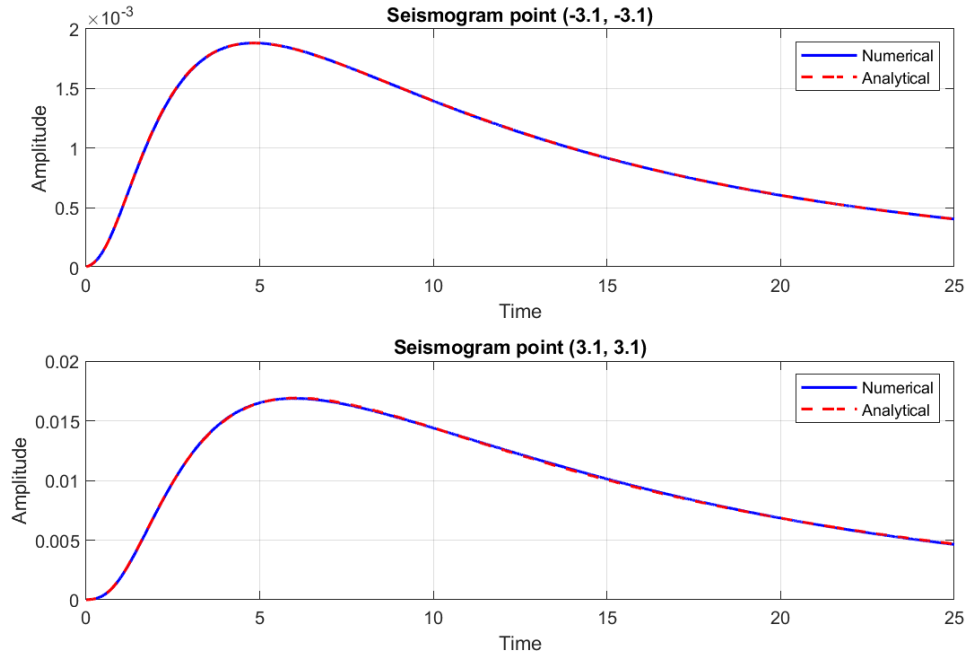


FIGURE 6. Time solution: RCSPML numerical v.s. analytical at two monitoring points: Top subplot: Point near bottom-left corner (x_1, y_1) , Bottom subplot: Point near top-right corner (x_2, y_2) .

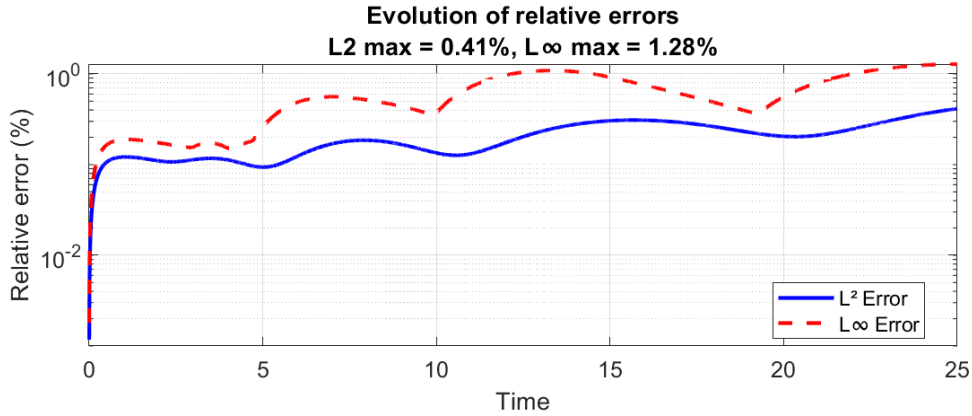


FIGURE 7. Semi-log plot over time: L^2 / L^∞ relative errors in percentage (%) of RCSPML numerical solution w.r.t analytical solution.

9. REMARKS AND COMMENTS

- We have developed a new real coordinate stretching Perfectly Matched Layer (RCSPML) model for the anisotropic advection-diffusion equation with cross derivative.
- The RCSPML model is well-posed and very simple to handle numerically. It is free of auxiliary variables. Moreover, it allows to study analytically the Green kernels decomposition: Incident - Reflected and transmitted ones, directly as functions of the layer parameters.
- Numerical tests were successfully validated with an initial Gaussian pulse (distributed) which are more convincing than experiments with a localized point source. Relative L^2 and L^∞ errors w.r.t exact solution perfectly matched the result with a reference solution.
- For isotropic problems, the model readily extends to three or higher dimensions, leveraging the multiplicative property of the heat kernel.
- Namely, for the time-fractional advection-diffusion equation [17], the extension is technical but possible, as far as there is no time frequency ω in the real coordinate transformation.
- Our model is inherently designed for diffusion phenomena dominated by evanescent modes, suggesting straightforward extension to parabolic systems. However, its applicability to mixed (hyperbolic-parabolic) systems—particularly when the parabolic part is non-dominant—is not explored in this paper.

ACKNOWLEDGMENT

The author thanks the referees for their helpful suggestions and comments on the last version of the draft.

This work has been partially supported by the Ministry of Higher Education and Scientific Research of Algeria, GEANLAB of the University of Oran 1 Ahmed Ben Bella, and LMSA Laboratory of the University of Science and Technology Oran Mohamed Boudiaf (USTOMB).

REFERENCES

1. Berenger, J.-P. (1994). A perfectly matched layer for the absorption of electromagnetic waves. *Journal of Computational Physics*, 114(2), 185–200. <https://doi.org/10.1006/jcph.1994.1159>
2. Berenger, J.-P. (1996). Three-dimensional perfectly matched layer for the absorption of electromagnetic waves. *Journal of Computational Physics*, 127(2), 363–379. <https://doi.org/10.1006/jcph.1996.0181>
3. Colonius, T. (2004). Modeling artificial boundary conditions for compressible flow. In *Annual Review of Fluid Mechanics* (Vol. 36, pp. 315–345). Annual Reviews. <https://doi.org/10.1146/annurev.fluid.36.050802.121930>
4. Dea, J. R. (2014). A Higdon-like non-reflecting boundary condition for the Klein–Gordon equation with evanescent waves. *Wave Motion*, 51(2), 256–265. <https://doi.org/10.1016/j.wavemoti.2013.08.002>
5. Ditkowski, A., & Gottlieb, D. (2003). On the Engquist Majda absorbing boundary conditions for hyperbolic systems. In *Recent Advances in Scientific Computing and Partial Differential*

- Equations* (pp. 55–72). American Mathematical Society. <https://doi.org/10.1090/conm/330/05884>
6. Dubach, E. (1996). Artificial boundary conditions for diffusion equations: Numerical study. *Journal of Computational and Applied Mathematics*, 70(1), 127–144. [https://doi.org/10.1016/0377-0427\(95\)00138-6](https://doi.org/10.1016/0377-0427(95)00138-6)
 7. Ehrhardt, M. (2010). Absorbing boundary conditions for hyperbolic systems. *Numerical Mathematics: Theory, Methods and Applications*, 3(3), 295–337. <https://doi.org/10.4208/nmtma.2010.33.3>
 8. Ehrhardt, M., & Mickens, R. E. (2006). Discrete artificial boundary conditions for the Black-Scholes equation of American options. *Matheon Preprint, Technische Universität Berlin*. <https://opus4.kobv.de/opus4-matheon/frontdoor/index/index/docId/320>
 9. Engquist, B., & Majda, A. (1977). Absorbing boundary conditions for the numerical simulation of waves. *Mathematics of Computation*, 31(139), 629–651. <https://doi.org/10.2307/2005997>
 10. Lewis, R. W., & Morgan, K. (Eds.). (1989). *Numerical Methods in Thermal Problems: Proceedings of the Sixth International Conference Held in Swansea, U.K., on July 3rd-July 7th, 1989*. Pineridge Press. <https://isbsearch.org/isbn/9780906674697>
 11. Halpern, L. (1986). Artificial boundary conditions for the linear advection-diffusion equation. *Mathematics of Computation*, 46(174), 425–438. <https://doi.org/10.2307/2007985>
 12. Halpern, L., & Rauch, J. (1995). Absorbing boundary conditions for diffusion equations. *Numerische Mathematik*, 71(2), 185–224. <https://doi.org/10.1007/s002110050141>
 13. Halpern, L. (2007). Optimized sponge layers, optimized Schwarz waveform relaxation algorithms for convection-diffusion problems and best approximation. In *Domain Decomposition Methods in Science and Engineering XVI* (pp. 299–306). Springer. https://doi.org/10.1007/978-3-540-34469-8_35
 14. Hu, F. Q., Li, X. D., & Lin, D. K. (2008). Absorbing boundary conditions for nonlinear Euler and Navier-Stokes equations based on the perfectly matched layer technique. *Journal of Computational Physics*, 227(9), 4398–4424. <https://doi.org/10.1016/j.jcp.2008.01.010>
 15. Jacques, M., & Wilk, O. (2021). High-order absorbing boundary condition, domain decomposition method and stratified dispersive wave model. *Wave Motion*, 106, 102806. <https://doi.org/10.1016/j.wavemoti.2021.102806>
 16. Joly, P., & Nédélec, J.-C. (1989). Pseudo-transparent boundary conditions for the diffusion equation. Part I. *Mathematical Methods in the Applied Sciences*, 11(6), 725–758. <https://doi.org/10.1002/mma.1670110602>
 17. Kunasegaran, P., & Mat Isa, Z. (2025). Analytical solution of two-dimensional fractional advection-diffusion equation with instantaneous source and time-varying coefficients. *Gulf Journal of Mathematics*, 21(1), 470–485. <https://doi.org/10.56947/gjom.v21i1.3403>
 18. Lantos, N., & Nataf, F. (2010). Perfectly matched layers for the heat and advection-diffusion equations. *Comptes Rendus Mathématique*, 348(13), 781–785. <https://doi.org/10.1016/j.crma.2010.05.004>
 19. Tsynkov, S. V. (1998). Numerical solution of problems on unbounded domains: A review. *Applied Numerical Mathematics*, 27(4), 465–532. [https://doi.org/10.1016/S0168-9274\(98\)00025-7](https://doi.org/10.1016/S0168-9274(98)00025-7)

¹ DEPARTMENT OF MATHEMATICS, UNIVERSITY OF SCIENCES AND TECHNOLOGIES OF ORAN - MOHAMED BOUDIAF - LABORATORY GEANLAB - UNIV-ORAN 1 ABB
 Email address: ahmed.benmeftah@univ-usto.dz

² DEPARTMENT OF MATHEMATICS, UNIVERSITY OF SCIENCES AND TECHNOLOGIES OF ORAN - MOHAMED BOUDIAF - LABORATORY LMSA - USTOMB
 Email address: nassima.khldi@univ-ust.dz, zohra.benkamra@univ-usto.dz